Polarization Dependence of Resonant X-Ray Emission Spectra in Early Transition Metal Compounds

Masahiko Matsubara, Takayuki Uozumi[1], Akio Kotani,
Yoshihisa Harada and Shik Shin

Institute for Solid State Physics, The University of Tokyo,
7-22-1 Roppongi, Minato-ku, Tokyo 106-8666
[1] College of Engineering, Osaka Prefecture University, Sakai 593-8531

We measure $2p \to 3d \to 2p$ resonant X-ray emission spectra (RXES) of d^0 system (ScF$_3$ and TiO$_2$) and analyze them by means of MX$_6$ (M=Sc or Ti, X=F or O, respectively) cluster model with full multiplet effects. We treat the whole RXES process as a coherent second order optical process and take the polarization dependence into account. The strong polarization dependence of the inelastic peak is clearly seen both in the experimental and calculated results. In order to clarify it, we investigate the detailed mechanism of the polarization dependent RXES by the total energy level diagram and the group theoretical consideration.

§1. Introduction

High-energy spectroscopy, such as X-ray photoemission spectroscopy (XPS) and X-ray absorption spectroscopy (XAS), has played an important role for a long time in the study of electronic structures of strongly correlated systems such as $3d$ transition metal (TM) compounds. In addition to these conventional first order optical processes, X-ray emission spectroscopy (XES), which is second order optical process, attracts much attention, because recent development of the synchrotron light source and the experimental technique enable it to be observed and it has the advantage of the charge neutrality, bulk sensitivity, and so on. In XES, a core electron is excited by the incident X-ray photon, and then the excited state decays by emitting an X-ray photon. When the core electron is excited near the threshold of the X-ray absorption, the XES is denoted by resonant XES (RXES), while it is denoted by normal XES (NXES) when the core electron is excited to the continuum well above the threshold. XES provides us with information complementary to XAS and XPS, the final states of which correspond to the intermediate states of RXES and NXES, respectively. Especially for RXES, we can select a specific intermediate state by tuning the incident photon energy, and obtain the spectra due to the transition from that intermediate state to final states.[1,2]

The synchrotron radiation has remarkable characteristic of polarization. It is clear that we can get more information from RXES by taking the polarization dependence into account, but to date it has not been utilized very effectively. It is very interesting to apply the polarization dependence to RXES of $3d$ TM compounds, which are extremely important because they indicate many interesting physical phenomena, for example, metal-insulator transition, high-T_c superconductivity, etc.

We have measured the spectra of Sc $2p \to 3d \to 2p$ RXES of ScF$_3$ and Ti $2p \to 3d \to 2p$ RXES of TiO$_2$ (rutile) (for the experiment of TiO$_2$, see also refs. 3, 4). We call these materials "d^0 system", since the ground state of the formally trivalent Sc and tetravalent Ti ions are described by the linear combinations of $3d^0$, $3d^1\underline{v}$, and $3d^2\underline{v}^2$ configurations due to the strong covalency hybridization with ligand states, where $3d^n\underline{v}^m$ denotes the state having n $3d$ electrons and m ligand holes. In these experiments, we take the incident photon polarization into account. The incident photon and the emitted photon are in the plane (scattering plane) normal to the sample surface, and the scattering angle is fixed to 90°. When the polarization vector of incident photon is parallel to the scattering plane, it is called the "depolarized" configuration, while when the polarization vector of incident photon is perpendicular to the scattering plane, it is called the "polarized" configuration (see Fig. 1). A dramatic change of the RXES spectra from the polarized to depolarized configurations will be shown for the d^0 systems.

Recently, Uozumi and co-workers have applied a cluster model to the analysis of M$_2$O$_3$ (M=Ti, V, Cr, Mn, Fe) compounds, and have shown that the spectra obtained by XPS, valence XPS, bremsstrahlung isochromat spectroscopy (BIS), etc. can be explained consistently, and they also analyzed the electronic structures of early TM compounds systematically.[5,6] In the present paper we analyze the Sc $2p \to 3d \to 2p$ RXES of ScF$_3$ and the Ti $2p \to 3d \to 2p$ RXES of TiO$_2$ taking the polarization dependence into account by following and extending their techniques appropriately. We compare the results with experimental ones, and clarify the origin of the polarization dependence of the RXES.

After describing the experimental results in §2, we give

the model and the formalism used in our calculation of RXES in §3, and show the calculated results in §4. In §5 we discuss the mechanism of the RXES in these d^0 systems and the origin of its polarization dependence.

§2.   Experimental Data

In this section we describe briefly the experimental method and show the experimental data of XAS and RXES for ScF$_3$ and TiO$_2$.

2.1   Experimental method

The experimental results were obtained by using a soft X-ray spectrometer[7] installed at the undulator beamline BL-2C[8] at Photon Factory, KEK. Synchrotron radiation was monochromatized using a varied-line spacing plain grating whose average groove density is 1000 lines/mm. The energy resolution of the incident photon was about 0.4 eV at 400 eV and 450 eV when we mea-
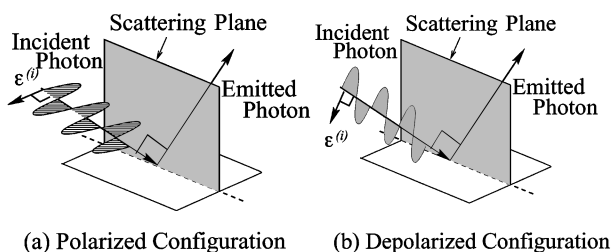

Fig. 1.   The schematic configuration of the experiment. (a) Polarized configuration: the polarization vector of the incident photon ($\varepsilon^{(i)}$) is perpendicular to the scattering plane. (b) Depolarized configuration: the polarization vector of the incident photon is parallel to the scattering plane. In both configurations, scattering angle is fixed to 90°.

sured RXES, and was about 0.1 eV when we measured absorption spectra. The spectrometer is Rowland mount type with a laminar grating whose radius and groove density are 5 m and 1200 lines/mm. The incident angle of the soft X-ray to the sample surface was about 70° to avoid the self-absorption effect.

The absorption and emission spectra were measured in the depolarized and polarized configurations. The RXES spectra were measured with the spectrometer resolution of 0.6 eV at 400 eV for ScF$_3$, and 0.6 eV at 450 eV for TiO$_2$ with a 20 μm incident slit width of the spectrometer, respectively.

2.2   ScF$_3$

In Fig. 2(a) Sc 2p total electron yield (TEY) spectrum of ScF$_3$ is shown. This spectrum has mainly four peaks, and in the higher energy region (above ~415 eV) we can see some weak satellite structures.

In Fig. 2(b), the spectra of Sc $2p \rightarrow 3d \rightarrow 2p$ RXES of ScF$_3$ are shown where both polarized (solid line) and depolarized (dots) spectra are plotted as a function of the difference between the incident and emitted photon energies (denoted by Raman shift), i.e. 0 eV corresponds to the elastic scattering (Rayleigh line). The indices from **a** to **h** indicate incident photon energies which correspond to those indicated in Fig. 2(a). The structures seen at ~13 eV, ~15 eV, etc. originate from the inelastic scattering. We can see the difference in the spectra of the polarized and depolarized configurations clearly. In the polarized configuration the elastic peak (at 0 eV) is greatly enhanced, so they are plotted with the intensity scale reduced by factor 20, while in the depolarized configuration the elastic peak is hardly seen. A more important point is that when incident photon energies are
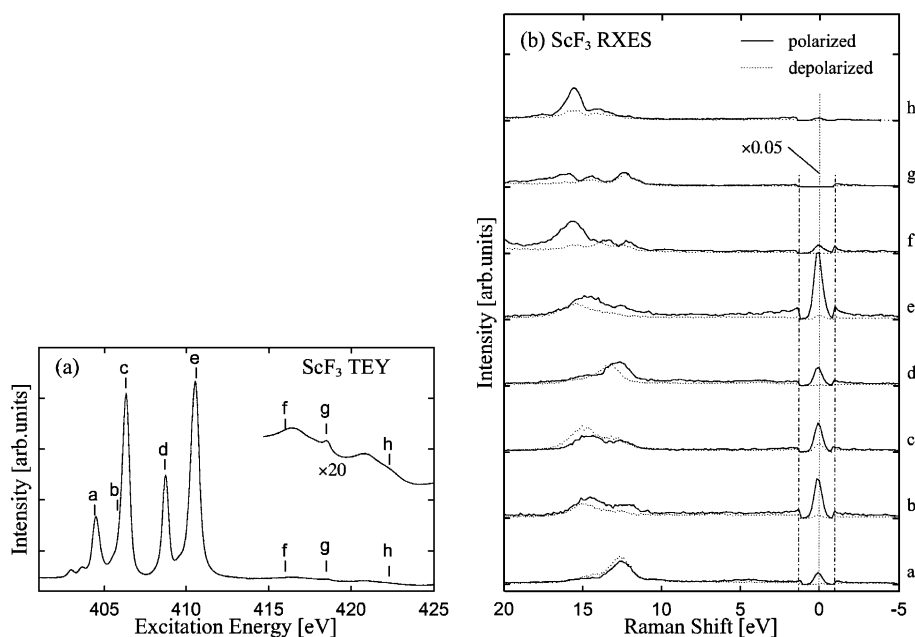

Fig. 2.   Experimental results of ScF$_3$. (a) Sc 2p XAS obtained by TEY. The vertical bars with indices represent the excitation energy. (b) Sc $2p \rightarrow 3d \rightarrow 2p$ RXES. This is plotted as a function of Raman shift. Both polarized (solid line) and depolarized (dots) spectra are plotted. The elastic peaks of both spectra are divided by 20.
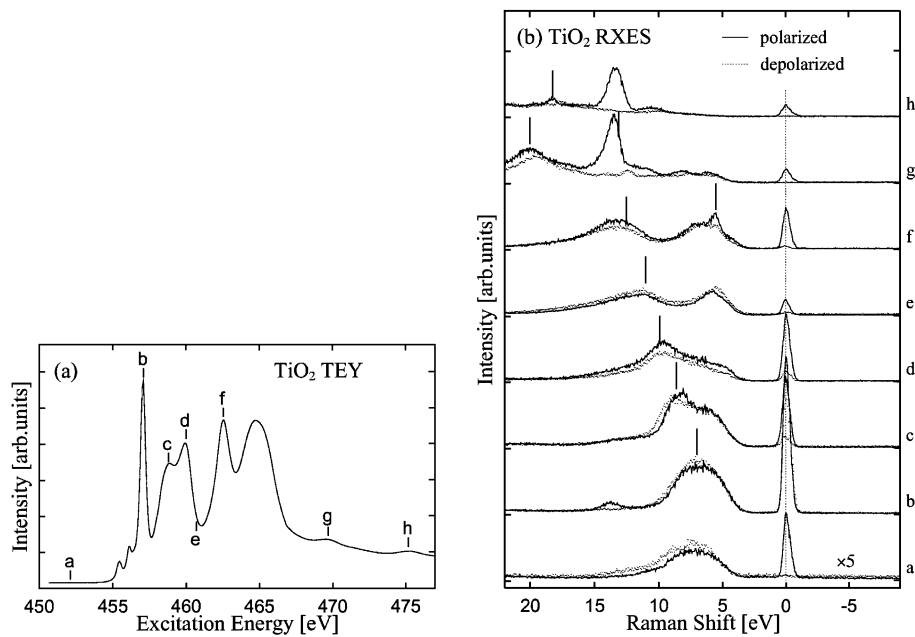
Fig. 3. Experimental results of TiO_2. (a) Ti $2p$ XAS obtained by TEY. The vertical bars represent the excitation energy. (b) Ti $2p \rightarrow 3d \rightarrow 2p$ RXES. This is plotted as a function of Raman shift. Both polarized (solid line) and depolarized (dots) spectra are plotted. The vertical bars are also plotted at the structures shifting to the lower energy side with the increase of incident photon energy.

set at **f** and **h** (satellite structures in XAS), the intensity of the inelastic peak around 16 eV is dramatically enhanced in the polarized configuration, while it is not enhanced in the depolarized configuration.

2.3 TiO₂

In Fig. 3(a), the Ti $2p$ TEY spectrum of TiO_2 is shown. As a whole its structure resembles that of ScF_3, that is, it has four main peaks between 455 eV and 465 eV (the second peak splits further into two peaks in more detail), and in the higher energy region there are some weak satellites.

In Fig. 3(b), the spectra of the Ti $2p \rightarrow 3d \rightarrow 2p$ RXES of TiO_2 are shown, in which both polarized (solid line) and depolarized (dots) spectra are plotted as a function of the Raman shift. In the polarized configuration, the elastic peak and the inelastic peak at about 14 eV are enhanced for the incident photon energies at the main peak and the satellite, respectively. However, these peaks are almost forbidden in the depolarized configuration. The inelastic spectra from 6 to 9 eV are allowed for both polarized and depolarized configurations. In addition to these structures, there are two broad peaks shifting to the higher energy side with the increase of the incident photon energy indicated with vertical bars, which are hardly seen in RXES of ScF_3, but seen in almost all $2p \rightarrow 3d \rightarrow 2p$ RXES of $3d$ transition metal compounds.[3,4]

§3. Model and Method of Spectral Analysis

3.1 Hamiltonian and spectral functions

We adopt the MX_6 (M=Sc, Ti, X=F, O) cluster model with O_h symmetry to analyze the experimental data.

The symmetry is exactly O_h for ScF_3, but for TiO_2 it is D_{2h}. The deviation from O_h in TiO_2, however, is small, so that we treat TiO_2 approximately as the O_h symmetry.

The Hamiltonian used in this calculation is given by

$$H = H_{atom} + H_v + H_{mix}, \qquad (3.1)$$

where

$$H_{atom} = \sum_\nu \varepsilon_d(\nu) d_\nu^\dagger d_\nu + \sum_\mu \varepsilon_p(\mu) c_\mu^\dagger c_\mu$$

$$+ U_{dd} \sum_{\nu > \nu'} d_\nu^\dagger d_\nu d_{\nu'}^\dagger d_{\nu'} - U_{dc} \sum_{\nu,\mu} d_\nu^\dagger d_\nu (1 - c_\mu^\dagger c_\mu)$$

$$+ H_{multiplet}, \qquad (3.2)$$

$$H_v = \sum_\nu \varepsilon_v v_\nu^\dagger v_\nu, \qquad (3.3)$$

$$H_{mix} = \sum_\nu V(\nu)(d_\nu^\dagger v_\nu + v_\nu^\dagger d_\nu). \qquad (3.4)$$

Here $d_\nu^\dagger(d_\nu)$, $c_\mu^\dagger(c_\mu)$, $v_\nu^\dagger(v_\nu)$ are electron creation (annihilation) operators for $3d$, core, X $2p$ orbitals, respectively. ν and μ denote the combined indices representing the spin (σ) and orbital (Γ) states, and Γ runs over t_{2g} and e_g, which are irreducible representations of O_h. The first term H_{atom} describes the M atomic state including the M $2p$ and $3d$ states. The second and third terms, H_v and H_{mix}, describe the X $2p$ molecular orbitals and the hybridization between the M $3d$ state and the X $2p$ molecular orbitals.

The first and second terms of H_{atom} denote the one particle energies for M $3d$ and $2p$ states, respectively, the third and fourth terms denote the Coulomb interac-

tion U_{dd} between $3d$ electrons and the attractive core-hole potential $-U_{dc}$ acting on the $3d$ electrons, respectively. The last term denotes the intra-atomic multiplet coupling originating from the multipole components of the Coulomb interaction between M $3d$ states and that between M $3d$ and $2p$ states. The spin-orbit interactions for M $3d$ and $2p$ states are also included in $H_{multiplet}$. The charge transfer (CT) energy Δ is defined as $\Delta = E(d^1\underline{v}) - E(d^0)$, where $\underline{v}$ denotes a hole in the X $2p$ orbital and $E(d^1\underline{v})$ and $E(d^0)$ denote the configuration averaged energies of $d^1\underline{v}$ and d^0 configurations, respectively. In this calculation we treat Δ, U_{dd}, U_{dc}, $V(e_g)$ $(= -2V(t_{2g})$, for simplicity), and the crystal field splitting energy $10Dq$ $(= \varepsilon(e_g) - \varepsilon(t_{2g}))$ as adjustable parameters. The Slater integrals F^k and G^k, and the spin-orbit coupling constant ζ are obtained by the atomic Hartree-Fock calculation, and then the Slater integrals are reduced to 85 %.

We describe the wave functions of the system by linear combinations of three different configurations. The ground state of the d^0 system is written as follows:

$$|g\rangle = c_0|d^0\rangle + c_1|d^1\underline{v}\rangle + c_2|d^2\underline{v}^2\rangle, \qquad (3.5)$$

where the three configurations are mixed with each other through the hybridization. The final state is also given by the same form as eq. (3.5). Similarly the intermediate state of the RXES (final state of XAS) can be described by linear combinations of $|d^1\underline{c}\rangle$, $|d^2\underline{v}\,\underline{c}\rangle$, and $|d^3\underline{v}^2\,\underline{c}\rangle$ as

$$|m\rangle = c_0'|d^1\underline{c}\rangle + c_1'|d^2\underline{v}\,\underline{c}\rangle + c_2'|d^3\underline{v}^2\,\underline{c}\rangle. \qquad (3.6)$$

The XAS spectrum is expressed as

$$F_{XAS}(\Omega) = \sum_m |\langle m|T_1|g\rangle|^2 \,\delta\,(\Omega - E_m + E_g), \quad (3.7)$$

where Ω is the incident photon energy, $|g\rangle$ and $|m\rangle$ are the ground state and the final states of XAS, respectively, with the energies E_g and E_m. We treat the whole RXES process as a coherent second order optical process, and hence for RXES we use the following formula:

$$F(\Omega, \omega) = \sum_f \left| \sum_m \frac{\langle f|T_2|m\rangle\langle m|T_1|g\rangle}{\Omega + E_g - E_m - i\Gamma_m} \right|^2$$
$$\times \delta\,(\Omega + E_g - \omega - E_f), \qquad (3.8)$$

where $|g\rangle$ and $|m\rangle$ are the same as those in eq. (3.7) and $|f\rangle$ denotes the final states of RXES with energies E_f. T_1 and T_2 are the electric dipole transition operators. The incident and emitted photon energies are represented by Ω and ω, respectively, and the Raman shift is defined by $\Omega - \omega$.

3.2 Polarization dependence

In order to take into account the polarization dependence of RXES, we transform eq. (3.8) into a suitable form. Using the polarization vector $\boldsymbol{\varepsilon} = (\varepsilon_x, \varepsilon_y, \varepsilon_z)$ and the normalized spherical harmonics

$$C_q^{(k)} = \sqrt{\frac{4\pi}{2k+1}}\, Y_{kq}, \qquad (3.9)$$

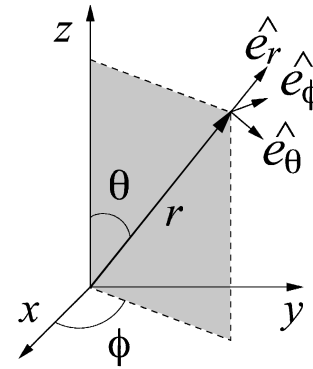the electric dipole transition operator T, either of T_1 or

Fig. 4. Spherical coordinates used in this calculation. x, y, z are fixed at the material. $\hat{\boldsymbol{e}}_r$, $\hat{\boldsymbol{e}}_\theta$, $\hat{\boldsymbol{e}}_\phi$ are the primitive vectors of r, θ, ϕ, respectively.

T_2, is written, apart from an unimportant factor, as follows:

$$T = -\sqrt{\frac{1}{2}}\,(\varepsilon_x - i\varepsilon_y)\,C_1^{(1)}$$
$$+ \sqrt{\frac{1}{2}}\,(\varepsilon_x + i\varepsilon_y)\,C_{-1}^{(1)} + \varepsilon_z\,C_0^{(1)}. \qquad (3.10)$$

It is convenient to represent the whole system by spherical coordinates (see Fig. 4). The z-axis is set to one of the M-X axes of the MX_6 cluster, and included in the scattering plane (shaded plane). When the incident photon is in the depolarized configuration, the incident polarization vector $\boldsymbol{\varepsilon}^{(i)}$ is in the scattering plane, i.e. $\boldsymbol{\varepsilon}^{(i)} \parallel \hat{\boldsymbol{e}}_\theta$, where $\hat{\boldsymbol{e}}_\theta$ is the primitive vector of θ, while when it is in the polarized configuration it is perpendicular to the scattering plane, i.e. $\boldsymbol{\varepsilon}^{(i)} \perp \hat{\boldsymbol{e}}_\theta$. In the depolarized configuration $\boldsymbol{\varepsilon}^{(i)}$ is described by

$$\begin{pmatrix} \varepsilon_x^{(i)} \\ \varepsilon_y^{(i)} \\ \varepsilon_z^{(i)} \end{pmatrix} = \begin{pmatrix} \cos\theta\cos\phi \\ \cos\theta\sin\phi \\ -\sin\theta \end{pmatrix}, \qquad (3.11)$$

while in the polarized configuration $\boldsymbol{\varepsilon}^{(i)}$ is

$$\begin{pmatrix} \varepsilon_x^{(i)} \\ \varepsilon_y^{(i)} \\ \varepsilon_z^{(i)} \end{pmatrix} = \begin{pmatrix} -\sin\phi \\ \cos\phi \\ 0 \end{pmatrix}. \qquad (3.12)$$

The electric dipole transition operator T_1 of the two cases are written as follows:

$$T_1 = -\sqrt{\frac{1}{2}}\,\cos\theta\,e^{-i\phi}\,C_1^{(1)} + \sqrt{\frac{1}{2}}\,\cos\theta\,e^{i\phi}\,C_{-1}^{(1)}$$
$$- \sin\theta\,C_0^{(1)} \quad \text{(depolarized)}, \qquad (3.13)$$

$$T_1 = \sqrt{\frac{1}{2}}\,i\,e^{-i\phi}\,C_1^{(1)} + \sqrt{\frac{1}{2}}\,i\,e^{i\phi}\,C_{-1}^{(1)}$$
$$\text{(polarized)}. \quad (3.14)$$

Furthermore, since the spectral shape in O_h symmetry is independent of the direction of incident photon when the scattering angle is fixed at 90°, we assume the grazing incidence along x-axis, i.e. $\theta = 90°$, and $\phi = 0°$, for

simplicity.

In the X-ray emission process, we average over all the polarizations of the emitted photon because the polarization of the emitted photon is not detected in experimental measurements.

After all, we can rewrite eq. (3.8) as follows:

$$F(\Omega, \omega)$$
$$= \sum_f \left| \sum_{q=\pm 1} \sum_m \frac{\langle f|C_q^{(1)}|m\rangle \langle m|C_0^{(1)}|g\rangle}{\Omega + E_g - E_m - i\Gamma_m} \right|^2$$
$$\times \, \delta\left(\Omega + E_g - \omega - E_f\right) \quad \text{(depolarized)}, \quad (3.15)$$

$$F(\Omega, \omega)$$
$$= \sum_f \left| \sum_{q,q'=\pm 1} \sum_m \frac{\langle f|C_q^{(1)}|m\rangle \langle m|C_{q'}^{(1)}|g\rangle}{\Omega + E_g - E_m - i\Gamma_m} \right|^2$$
$$\times \, \delta\left(\Omega + E_g - \omega - E_f\right) \quad \text{(polarized)}. \quad (3.16)$$

§4. Numerical Results

In this section we show the calculated results. The parameter values used in this calculation are shown in Table I. In addition, we take into account the effect of configuration-dependent hybridization[11, 12] by introducing two factors R_c and R_v: Since M $3d$ wave function is contracted when a $2p$ hole is created, the hybridization strength $V(\Gamma)$ between $3d^0$ and $3d^1\underline{v}$ configurations is reduced to $R_c V(\Gamma)$ between $d^1\underline{c}$ and $d^2\underline{v}\,\underline{c}$ configurations. Meanwhile, the hybridization between $3d^1\underline{v}$ and $3d^2\underline{v}^2$ is enhanced to $V(\Gamma)/R_v$ because the $3d$ wave function is more extended with increasing $3d$ electron number (R_c

Table I. Solid state parameters (eV) used in the calculation.

Compound	Δ	U_{dd}	$V(e_g)$	U_{dc}	$10Dq$	R_c	R_v
ScF$_3$	9.0	4.0	4.2	5.5	1.0	0.75	0.9
TiO$_2$	2.98	4.0	3.4	6.0	1.7	0.8	0.9

and R_v being both less than unity).

XAS spectra are convoluted with the Lorentzian and Gaussian functions with the half width at half maximum (HWHM) $\Gamma_L = 0.1\,\text{eV}$ and $\Gamma_G = 0.5\,\text{eV}$, respectively, while all RXES spectra are convoluted with only the Gaussian functions with the same HWHM value as XAS.

4.1 ScF$_3$

In Fig. 5(a), we show the calculated result of XAS. The spectrum is split into two states, t_{2g} and e_g due to the crystal field, and each state is split due to the spin-orbit interaction of the Sc $2p$ core level. Thus, the main XAS structure consists of four peaks. In addition to them, there are very weak satellites on the higher energy side of the main structure. This result is in good agreement with experimental one (see Fig. 2(a)).

In Fig. 5(b), we show the calculated result of RXES. Both spectra in the polarized (solid line) and depolarized (dotted line) configurations are plotted as a function of the Raman shift. The indices from **a** to **h** indicate the incident photon energies which correspond to those indicated in Fig. 5(a). We can see that in the polarized configuration the elastic peak at 0 eV and the inelastic peak around 16 eV are greatly enhanced when incident photon energy is set to the main peak and the satellite
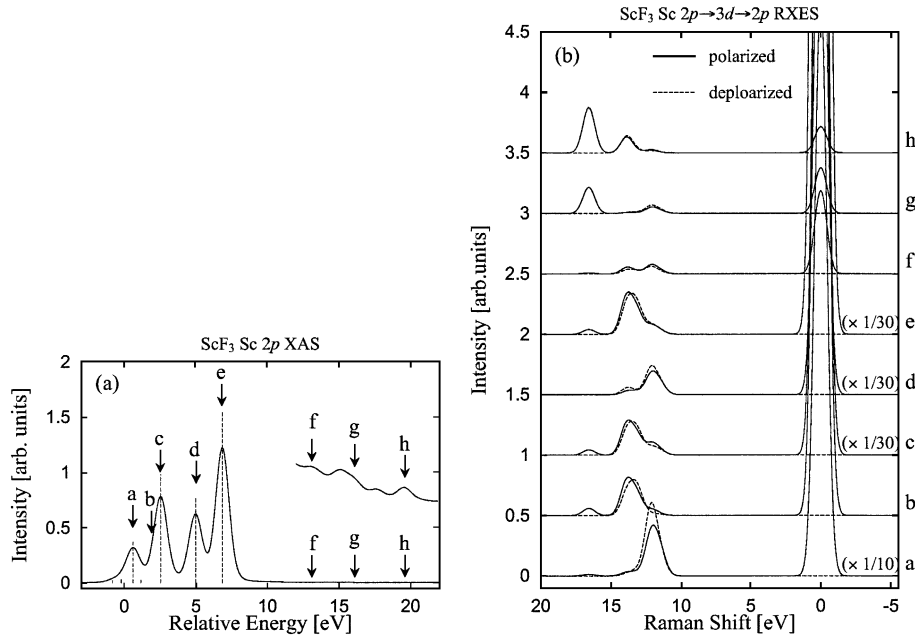

Fig. 5. Calculated results of ScF$_3$. (a) Sc $2p$ XAS spectrum. (b) Sc $2p \to 3d \to 2p$ RXES. The polarized spectra are plotted by solid line, while the depolarized spectra are plotted by dotted line. These are both plotted as a function of Raman Shift. The indices from **a** to **h** correspond to those indicated in XAS spectrum, and they are the incident photon energies of the RXES. Spectra **a**, **c**, **d**, **e** are divided by factor 10, 30, 30, 30, respectively. When the incident photon energies are fixed at the satellite of XAS (i.e. **g**, **h**), the polarized spectra around 16 eV are dramatically enhanced, whereas the depolarized ones not enhanced.
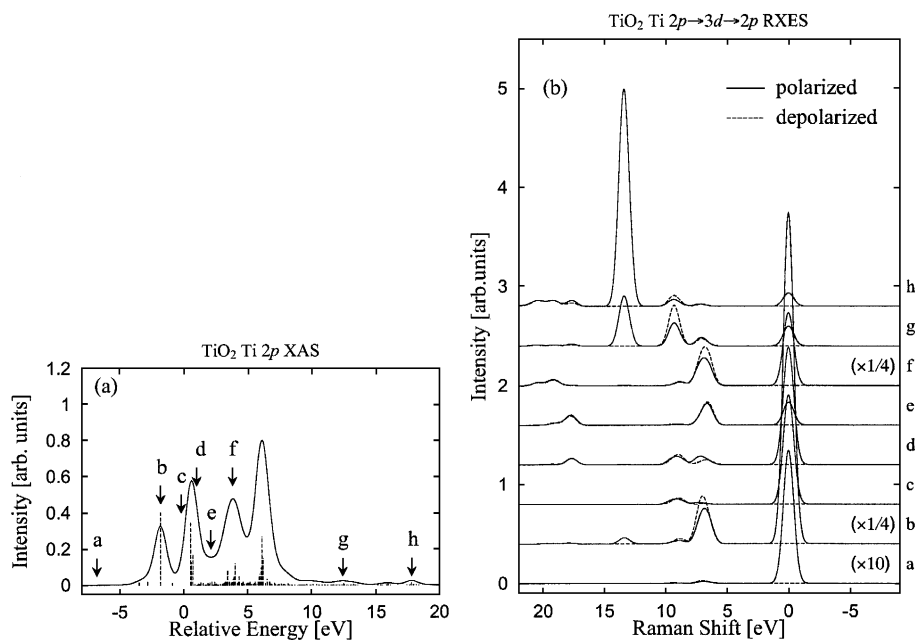
Fig. 6. Calculated results of TiO$_2$. (a) Ti $2p$ XAS. (b) Ti $2p \rightarrow 3d \rightarrow 2p$ RXES. The polarized spectra are plotted by solid line, while the depolarized spectra are plotted by the dotted line. Indices from **a** to **h** denote the incident photon energies. Spectrum **a** is multiplied by 10, and spectra **b**, **f** are divided by factor 4. When the incident photon energies are fixed at the satellite of XAS (i.e. **g**, **h**), the polarized spectra are also dramatically enhanced, whereas the depolarized ones not enhanced.

of the XAS, respectively. On the other hand, both 0 eV and 16 eV peaks are forbidden in the depolarized configuration. In addition to them, we can see two peaks at about 12 eV and 14 eV in both polarized and depolarized configurations. When the incident photon energy is set to the t_{2g} excited state of XAS, for example for **a** and **d**, the lower energy peak (at 12 eV) is enhanced, whereas for the e_g excited state, for example for **c** and **e**, the higher energy peak (at 14 eV) is enhanced. These results are in good agreement with experimental data (Fig. 2(b)).

4.2 TiO$_2$

In Fig. 6(a), the calculated result of XAS is shown. Similarly to ScF$_3$, the main XAS structure consists of four peaks due to the spin-orbit splitting and the crystal field splitting, and weak satellite structures are seen on the higher energy side of the main structure. However some difference between the calculated and experimental results is seen. The second peak of the main structure is split into two in the experiment, but only one peak is seen in the calculation. This discrepancy is due to our approximation that the local symmetry around Ti is not D_{2h} but O_h, as mentioned in §3. The lower symmetry calculation reproduces this splitting correctly.[13]

In Fig. 6(b), we show the calculated results of RXES. In the polarized configuration, the elastic peak and the inelastic peak around 14 eV are greatly enhanced when the incident photon energy is set to the main peak and the satellite of the XAS, respectively, whereas they are forbidden in the depolarized configuration. The inelastic peaks at about 7 eV and 9 eV are allowed in both polarized and depolarized configurations. The 7 eV peak is enhanced when the incident photon energy is set to the
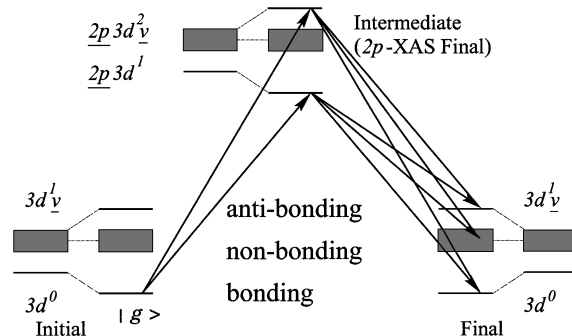

Fig. 7. Total energy level scheme of $2p \rightarrow 3d \rightarrow 2p$ RXES of d^0 system. Detailed mechanism is explained in the text.

t_{2g} excited state of XAS, while the 9 eV peak is enhanced when it is set to the e_g excited state.

We cannot reproduce the peaks shifting to the higher energy side as the incident photon energy is increased (indicated by the vertical bars in Fig. 3(b)). Some discussion on these peaks will be given in §5.

§5. Discussion

In the case of d^0 system, both the experimental and calculated results show the conspicuous difference between the RXES spectra in the polarized and depolarized configurations. Here we discuss the mechanism of the RXES and its polarization dependence. We show the total energy level scheme of d^0 system in Fig. 7, where only the two lowest energy configurations are considered and the spin-orbit splitting of the $2p$ states and the crystal field splitting of the $3d$ states are neglected for simplicity.

The initial and final states consist of three types of electronic states: the bonding and antibonding states between d^0 and $d^1\underline{v}$ configurations and nonbonding $d^1\underline{v}$ states. The energy separation between the bonding and antibonding states ($E_{diff}^{(g)}$) is estimated as follows:

$$E_{diff}^{(g)} = \sqrt{\Delta^2 + 4V_{eff}^{\,2}}, \qquad (5.1)$$

where V_{eff} is the effective hybridization expressed as $\sqrt{6V(t_{2g})^2 + 4V(e_g)^2}$. The ground state is the bonding state and the antibonding state is located about $16\,\mathrm{eV}$ and $14\,\mathrm{eV}$ above the bonding state for ScF_3 and TiO_2, respectively. The nonbonding states are located close to the antibonding state for ScF_3, while almost in the middle of the antibonding and bonding states for TiO_2, because the charge transfer energy Δ of ScF_3 is much larger than that of TiO_2.

The intermediate states are the bonding and antibonding states between $\underline{2p}d^1$ and $\underline{2p}d^2\underline{v}$ configurations, and the $\underline{2p}d^2\underline{v}$ nonbonding states. The energy separation between the bonding and antibonding states ($E_{diff}^{(m)}$) is estimated as follows:

$$E_{diff}^{(m)} = \sqrt{(\Delta - U_{dc})^2 + 4(Rc\,V_{eff}/Rv)^2}. \quad (5.2)$$

The main peak and the satellite of M $2p$ XAS correspond to the bonding and antibonding intermediate states, respectively, whose energy separation is about $13\,\mathrm{eV}$ for ScF_3 and about $12\,\mathrm{eV}$ for TiO_2. The intensity of the satellite is very weak due to the phase cancellation between the wave functions of the ground and intermediate states. The transition to the nonbonding states is almost forbidden.

By the radiative transition from the intermediate states, each of the final states (bonding, antibonding and nonbonding states) can be reached. The RXES spectra of the elastic peak and the $16\,\mathrm{eV}$ (for ScF_3) inelastic peak ($14\,\mathrm{eV}$ for TiO_2) correspond, respectively, to the

bonding and antibonding final states, while the inelastic spectra in between them correspond to the nonbonding final states. When the incident photon energy is fixed at the main peak of $2p$ XAS, which corresponds to the bonding intermediate states, the transition to the bonding final state is strong, but that to the antibonding final state is very weak. For the transition to the nonbonding final states, if the incident photon energy is tuned to the $t_{2g}(e_g)$ peak of XAS, the nonbonding $d^1\underline{v}$ final states with $d = t_{2g}(e_g)$ is enhanced due to the overlap of wave functions in the intermediate and final states. On the other hand, when the incident photon energy is fixed at the satellite of $2p$ XAS, which corresponds to the antibonding intermediate state, the transition to the antibonding final state is strong, but that to the bonding and nonbonding states are weak.

The polarization dependence in RXES is explained by a group theoretical consideration. According to the Wigner-Eckart theorem, the optical transition matrix element is described as the Clebsch-Gordan (CG) coefficient:

$$\langle \alpha\Gamma\gamma | T_{\overline{\gamma}}(\overline{\Gamma}) | \alpha'\Gamma'\gamma' \rangle \propto \langle \Gamma\gamma | \Gamma'\gamma'\overline{\Gamma}\overline{\gamma} \rangle. \quad (5.3)$$

Here α (α') denotes the electron configuration, Γ (Γ', $\overline{\Gamma}$) the irreducible representation of the group, and γ (γ', $\overline{\gamma}$) denotes the base of irreducible representations. Because only the electric dipole transition is considered here, $\overline{\Gamma}$ is T_{1u}. The transition occurs only when the CG coefficient is nonzero. Some CG coefficients in the O_h symmetry are given in Tables II and III. The ground state of the d^0 system is an A_{1g} state. In the depolarized and polarized configurations, as shown in §3, the polarization of the incident photon is in the z and y directions, respectively, where the y direction is taken to be normal with the scattering plane (zx plane), so that the possible basis of T_{1u} is z and y, respectively. Therefore the transition from the ground state to the intermediate state is allowed only when $\langle \Gamma\gamma | T_z(T_{1u}) | A_{1g} \rangle$ (depolarized configuration) and $\langle \Gamma\gamma | T_y(T_{1u}) | A_{1g} \rangle$ (polarized configuration) are nonzero.

From the Table II the absorption process (transition from the ground state to the intermediate state) is limited as follows:

$$A_{1g} \otimes T_{1u,z} = T_{1u,z} \qquad \text{(depolarized)}, \quad (5.4)$$

$$A_{1g} \otimes T_{1u,y} = T_{1u,y} \qquad \text{(polarized)}. \quad (5.5)$$

In the transition from the intermediate to final states, which is also the dipole transition, the polarization of

Table II. The Clebsch-Gordan coefficients $\langle \Gamma'\gamma'\overline{\Gamma}\overline{\gamma} | \Gamma\gamma \rangle$ of $A_1 \otimes T_1$. $\{e_1\} = \{1\}$ is the basis of A_1 and $\{\alpha,\beta,\gamma\} = \{x,y,z\}$ are the bases of T_1, respectively.

$\Gamma'\gamma'$	$\overline{\Gamma}\overline{\gamma}$	$\Gamma\gamma$		
		$T_1\alpha$	$T_1\beta$	$T_1\gamma$
	$T_1\alpha$	1		
$A_1 e_1$	$T_1\beta$		1	
	$T_1\gamma$			1

Table III. The Clebsch-Gordan coefficients $\langle \Gamma'\gamma'\overline{\Gamma}\overline{\gamma} | \Gamma\gamma \rangle$ of $T_1 \times T_1$. $\{e_1 = 1\}$ is the basis of A_1, $\{u,v\} = \{3z^2 - r^2, \sqrt{3}(x^2 - y^2)\}$ are the bases of E, $\{\alpha,\beta,\gamma\} = \{x,y,z\}$ are the bases of T_1, and $\{\xi,\eta,\zeta\} = \{yz, zx, xy\}$ are the bases of T_2, respectively.

$\Gamma'\gamma'$	$\overline{\Gamma}\overline{\gamma}$	$\Gamma\gamma$								
		$A_1 e_1$	Eu	Ev	$T_1\alpha$	$T_1\beta$	$T_1\gamma$	$T_2\xi$	$T_2\eta$	$T_2\zeta$
$T_1\beta$	$T_1\alpha$						$1/\sqrt{2}$			$-1/\sqrt{2}$
	$T_1\beta$	$-1/\sqrt{3}$	$1/\sqrt{6}$	$1/\sqrt{2}$						
$T_1\gamma$	$T_1\alpha$					$-1/\sqrt{2}$			$-1/\sqrt{2}$	
	$T_1\beta$				$1/\sqrt{2}$		$-1/\sqrt{2}$			

the emitted photon is in the x and y directions, i.e. the possible basis of T_{1u} is x and y. Similarly to the absorption process, from the Table III the emission process (transition from the intermediate to final states) is limited as follows:

$$T_{1u,z} \otimes T_{1u,\gamma} = T_{1g}, T_{2g} \qquad (\gamma = \{x,y\}), \quad (5.6)$$

$$T_{1u,y} \otimes T_{1u,\gamma} = A_{1g}, E_g, T_{1g}, T_{2g} \quad (\gamma = \{x,y\}). \quad (5.7)$$

Hence, in the depolarized configuration the final states of T_{1g} and T_{2g} are allowed, while in the polarized configuration those of A_{1g}, E_g, T_{1g} and T_{2g} are allowed. It is to be noted that the bonding and antibonding final states are in the same irreducible representation A_{1g}, while the nonbonding states which do not couple with A_{1g} state are in the irreducible representations $T_{1g}, T_{2g}, E_g, \cdots$ (which originate from the product of the symmetries d and $\underline{v}$). Therefore, the elastic peak and the antibonding inelastic peak are allowed (forbidden) for the polarized (depolarized) configuration, while the nonbonding inelastic peaks are allowed for both polarized and depolarized configurations.

In the rest of this section, we discuss the origin of the spectra indicated by the vertical bars in Fig. 3(b). The energy position of these bars changes almost proportionally to the change of the incident photon energy, so that the emitted photon energy is almost independent of the incident photon energy, similarly to NXES spectra. In this sense, we call these spectra "NXES-like spectra". Recently Idé and Kotani calculated RXES with a one-dimensional d-p model (a simplified version of the d^0 system) with multi-TM sites.[10] They showed that NXES-like spectra are absent in the cluster with a single TM site, but for larger clusters NXES-like spectra occur to some extent above the XAS threshold because of the existence of spatially extending XAS final states (RXES intermediate states) as a result of multi-TM sites effect. Therefore, in order to reproduce the NXES-like spectra of TiO_2, it would be necessary to extend the cluster size to that larger than the present TiO_6 cluster.

Acknowledgment

1) S. Tanaka, K. Okada and A. Kotani: J. Phys. Soc. Jpn. **60** (1991) 3893.
2) J. P. Hill, C.-C. Kao, W. A. Caliebe, M. Matsubara, A. Kotani, J. L. Peng and R. L. Greene: Phys. Rev. Lett. **80** (1998) 4967.
3) Y. Tezuka, S. Shin, A. Agui, M. Fujisawa and T. Ishii: J. Phys. Soc. Jpn. **65** (1996) 312.
4) Y. Harada, T. Kinugasa, R. Eguchi, S. Shin, M. Matsubara and A. Kotani: submitted to Phys. Rev. B.
5) T. Uozumi, K. Okada and A. Kotani: J. Electron Spectrosc. Relat. Phenom. **78** (1996) 103.
6) T. Uozumi, K. Okada, A. Kotani, R. Zimmermann, P. Steiner, S. Hüfner, Y. Tezuka and S. Shin: J. Electron Spectrosc. Relat. Phenom. **83** (1997) 9.
7) Y. Harada, H. Ishii, M. Fujisawa, Y. Tezuka, S. Shin, M. Watanabe, Y. Kitajima and A. Yagishita: J. Sync. Rad. **5** (1998) 1013.
8) M. Watanabe, A. Toyoshima, Y. Azuma, T. Hayaishi, Y. Yan and A. Yagishita: SPIE. **58** (1997) 3150.
9) M. Umeda, Y. Tezuka, S. Shin and A. Yagishita: Phys. Rev. B **53** (1996) 1783.
10) T. Idé and A. Kotani: J. Phys. Soc. Jpn. **67** (1998) 3621.
11) O. Gunnarsson and O. Jepsen: Phys. Rev. B **38** (1988) 3568.
12) K. Karlsson, O. Gunnarsson and O. Jepsen: J. Phys. C **4** (1992) 2801.
13) F. M. F. de Groot, J. C. Fuggle, B. T. Thole and G. A. Sawatzky: Phys. Rev. B **41** (1990) 928.
14) K. Okada and A. Kotani: J. Electron Spectrosc. Relat. Phenom. **62** (1993) 131.